Journal of Alloys and Compounds 506 (2010) 944–949

Contents lists available at ScienceDirect

Journal of Alloys and Compounds

journal homepage: www.elsevier.com/locate/jallcom

Synthesis of zinc oxide nanoparticles elaborated by microemulsion method

Özlem Altıntaş Yıldırım, Caner Durucan*

Department of Metallurgical and Materials Engineering, Middle East Technical University, 06531 Ankara, Turkey

ARTICLE INFO

Article history:
Received 11 January 2010
Received in revised form 12 July 2010
Accepted 13 July 2010
Available online 23 July 2010

Keywords:
Chemical synthesis
Nanostructured materials
Semiconductors

ABSTRACT

Zinc oxide (ZnO) nanoparticles were synthesized by a reverse microemulsion system formed from sodium bis(2-ethylhexyl)sulfosuccinate (Aerosol OT, or AOT):glycerol:n-heptane. The zinc precursor was zinc acetate dihydrate. The formation of ZnO nanoparticles was achieved by calcination of premature zinc glycerolate microemulsion product in air at 300, 400 and 500 °C. The crystal structure and the morphology of the ZnO nanoparticles were characterized by X-ray diffraction (XRD) and scanning electron microscopy (SEM). Thermal analysis was employed to reveal structural and chemical changes during calcination. Both surfactant concentrations – AOT – in the initial microemulsion formulation and the calcination temperature influenced the morphology and size of the ZnO nanoparticles. Low surfactant concentrations (5:5:90, AOT:glycerol:n-heptane, wt.%) resulted in formation of spherical ZnO nanoparticles. The average particle size increased from 15 ± 1 to 24 ± 1 nm with calcination temperature, but spherical morphology remained unchanged after all calcination treatments. The microemulsion system containing higher surfactant amount (30:5:65, AOT:glycerol:n-heptane, wt.%) resulted in rod-like ZnO nanostructures after calcination at 300 and 400 °C, with a diameter of 22 ± 3 and 28 ± 1 nm; and with a length of 66 ± 3 and 72 ± 1 nm, respectively. Further increase in the calcination temperature to 500 °C initiated rod-to-sphere shape transformation for the ZnO nanoparticles produced using this particular microemulsion formulation. For all ZnO microemulsion products, the photoluminescence measurements suggested a high defect concentration which increases with calcination temperature.

1. Introduction

Metal oxide nanoparticles have attracted considerable attention in many scientific and technological applications due to unique properties originating from their particle sizes in nano-scale. Zinc oxide (ZnO) is one of the well known semiconductor metal oxides with a wide direct band gap (3.37 eV) and large exciton binding energy (60 meV), providing various applications such as varistor [1,2], gas sensor [3–5], field emitter [6,7] and solar cell [8,9]. Due to the specific needs in these diverse applications, there has been a strong interest in the development of preparation methods enabling of production of ZnO nanostructures with well-controlled size and shape. Many methods ranging from gas-phase processes to solution routes have been intensively investigated for the synthesis of ZnO nanoparticles including solution precipitation [10,11], spray pyrolysis [12,13], hydrothermal synthesis [14–16] and sol–gel process [17–20].

Another versatile technique for synthesis of ZnO nanoparticles is microemulsion method. This synthesis method does not require any complex preparation procedure, sophisticated equipment and rigorous experimental conditions, but still providing possibilities in controlling the size and morphology of the ZnO powders in a size scale approaching to nanometers. Even though the product yield is low, narrow size distribution due to well-dispersed cage-like small reactors (5–100 nm) formed in uniform nucleation conditions, is the superior aspect of the ZnO nanoparticles obtained by microemulsion routes. Such low-dimensional uniform ZnO nanostructures offering size and morphology dependent tunable electrical and optical properties are of particular technological interest for applications such as quantum dots, UV-emission optoelectronic and lasing devices, as well as transparent conducting thin films.

There are numerous studies reporting preparation of spherical [21–24], rod shaped [25–28] or columnar [29] ZnO nanoparticles by reverse micellar systems or microemulsion-mediated systems. In most of these microemulsion-assisted routes, preparation of nanoparticles is achieved by direct recovery of the ZnO precipitates. Unfortunately, recovery of nanostructured microemulsion products by sedimentation results in aggregation of the ZnO precipitates either during sedimentation and/or subsequent calcination. It is therefore important to devise new methods for the preparation of homogeneous and mono dispersed ZnO nanoparticles by microemulsion routes.

In this study we attempted to use a modified microemulsion method for the synthesis of monodispersed ZnO nanoparticles. In this method, different than before mentioned reports ZnO

* Corresponding author. Tel.: +90 312 210 5840; fax: +90 312 210 2518.
E-mail address: cdurucan@metu.edu.tr (C. Durucan).

0925-8388/$ – see front matter © 2010 Elsevier B.V. All rights reserved.
doi:10.1016/j.jallcom.2010.07.125

nanoparticles are not directly produced in the microemulsion, but by thermal decomposition of a zinc-complex microemulsion product during subsequent calcination process. In our modified microemulsion process, glycerol was used as an internal phase of the reverse microemulsion (Aerosol OT:glycerol:heptane) in a procedure similar to that employed in preparation of ZnO nanoparticles in amorphous silica [23]. The specific objective of the present study is to determine the effects of surfactant concentration and calcination temperature on the size and morphology of the resultant ZnO nanoparticles. Characterization of ZnO nanoparticles was performed by combination of different analytical tools including X-ray diffraction (XRD), field emission scanning electron microscopy (FESEM), thermogravimetric (TGA), differential scanning calorimetric (DSC) analysis and photoluminescence (PL) spectroscopy. Herein, we present a microemulsion system to obtain size and shape-controlled crystalline ZnO nanoparticles and describe a correlation between the ZnO morphology, microemulsion formulation and calcination temperature for this system.

2. Material and experimental methods

2.1. Synthesis of ZnO nanoparticles

The synthesis of ZnO nanoparticles was carried out using reverse microemulsion system using sodium bis(2-ethylhexyl) sulfosuccinate ($C_{20}H_{37}NaO_7S$, Aerosol OT or AOT, 96%, Fluka) as the surfactant, glycerol ($C_3H_8O_3$, 87%, Riedel) as the polar phase and n-heptane (C_7H_{16}, extra pure, Riedel) as the non-polar phase. Zinc precursor was zinc acetate dihydrate ($C_4H_6O_4Zn{\cdot}2H_2O$, 99.5%, Riedel). All reagents were used without further purification. Two microemulsion formulations of different amount of surfactants were prepared. Microemulsion-I (hereafter referred as ME-I) composed of 5:5:90 (AOT:glycerol:n-heptane) in weight percentages. Microemulsion-II (here after referred as ME-II) with relatively more surfactant had a composition of 30:5:65 (AOT:glycerol:n-heptane) again in weight percentage. For obtaining the microemulsion, first two identical solutions were prepared with required amount of AOT dissolved in n-heptane at room temperature by stirring. After achieving complete dissolution, this solution was divided into glass containers and two separate AOT:n-heptane solutions, solution-A and solution-B, in equal parts were obtained. Then, half of the glycerol containing 0.5 M zinc acetate dihydrate was slowly added into solution-A under constant stirring. Similarly, rest of the glycerol containing 0.5 M sodium hydroxide (NaOH) solution was added into solution-B. NaOH was introduced as a catalyst. Both solutions were stirred at room temperature until they become completely transparent. Then, solution-B was slowly added into solution-A under constant stirring and the resulting mixture was further homogenized by refluxing at 60–70 °C for 24 h. At the end, the white solid powders were collected via centrifugation for 20 min at 10,000 rpm. The solid extracts were then washed three times with a mixture of 1:1 (vol%) methanol (CH_3OH, 99.9%, Riedel), and chloroform ($CHCl_3$, 99.8%, Sigma–Aldrich) solution by centrifugation at 10,000 rpm for 10 min. The obtained powders were dried at 100 °C for 1 h in an open atmosphere drying oven and in a vacuum dryer at room temperature for overnight. Finally, they were calcined in air atmosphere for 3 h at 300 °C, or 400 °C, or 500 °C.

2.2. Characterization

XRD analyses were performed for phase identification of microemulsion products in as-prepared (dried at 100 °C for 1 h) and after calcination treatments. A Rigaku D/Max-2000 PC diffractometer was employed in XRD analyses, using Cu-Kα radiation (λ = 1.54 Å) and X-ray source operating voltage of 40 kV in the 2θ range of 3–90° at a rate of 2°/min. The average crystallite size of the powders (D, in nm) was estimated by Scherrer's equation using the XRD line broadening method:

$$D = \frac{0.9\lambda}{\beta \cos\theta}$$

where, λ is the X-ray wavelength for CuKα, β is the full width in radians at half-maximum (FWHM) of the diffraction line and θ is the diffraction angle. (1 1 0) diffraction peak (at $2\theta \approx 56.614$) was chosen to determine a representative crystallite size for ZnO nanoparticles by employing the Scherrer equation.

The morphology and size of the ZnO particles was examined using a FEI Quanta 400F model FESEM. Samples were formed using a suspension of ZnO particles dispersed in distilled water by ultrasonic treatment. A few drops of dilute dispersion were deposited onto a carbon film taped to an aluminum grid and dried in air. FESEM examinations were performed without any conductive coating.

TGA and DSC experiments were carried out using Setaram SETSYS-16/18 on finely ground powders in air atmosphere between 30 and 700 °C with a heating rate of 5 °C/min.

PL measurements were conducted at room temperature with the HeCd laser (325 nm). The emitted light was collected by an MS 257 type monochromator and Hamamatsu CCD camera.

3. Results

Fig. 1a and b shows the XRD diffractograms of the microemulsion products for the formulations ME-I and ME-II, respectively. The diffractograms were obtained from powders in as-prepared condition and after calcination for 3 h at 300, 400 and 500 °C. For both microemulsion systems, the XRD patterns of the particles in as-prepared condition coincide with that of zinc glycerolate (Zn-Gly, with JCPDS card No. 23-1975) and no other crystalline phase besides Zn-Gly was observed. After calcination the intermediate microemulsion precursor, Zn-Gly, decomposes to crystalline ZnO (hexagonal wurtzite structure, with JCPDS card No. 36-1451). For ME-I, this decomposition completes at 300 °C. ZnO obtained in ME-II microemulsion still contained some residual Zn-Gly after calcination at 300 °C. For both systems calcination at 400 or 500 °C results in phase pure crystalline ZnO powder. Another distinction between XRD patterns of ZnO particles synthesized in ME-I and ME-II system is the difference in relative intensities of the certain

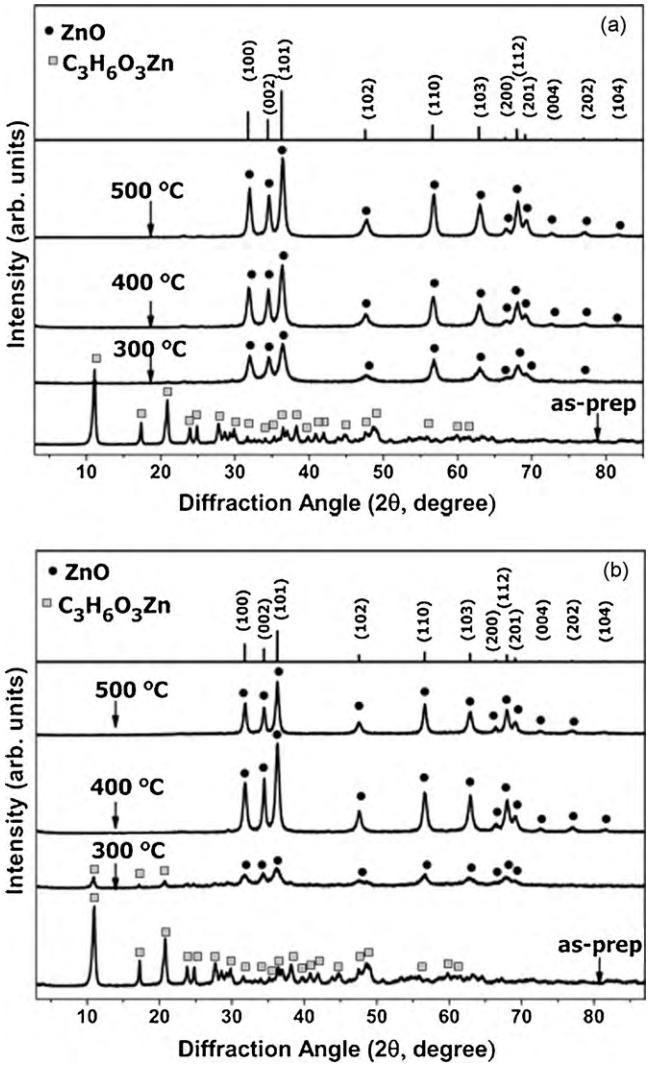

Fig. 1. XRD patterns of microemulsion products in as-prepared condition (for precursor zinc-complex) and after 3 h calcination in air at different temperatures for two microemulsion formulations: (a) ME-I and (b) ME-II. The inset shows the relative intensities of the standard ZnO (with JCPDS card No. 36-1451) diffraction pattern.

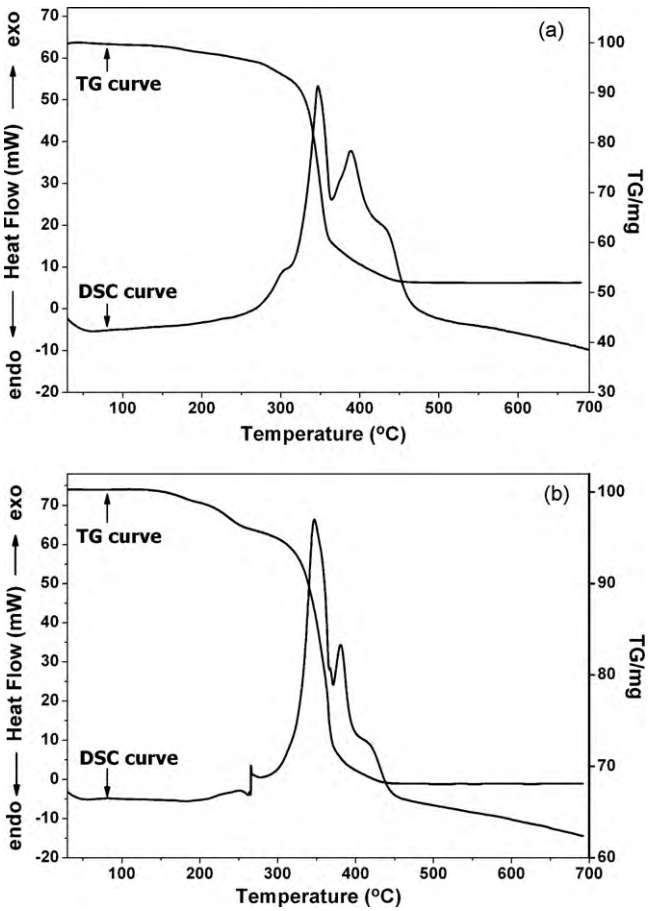

Fig. 2. TGA and DSC plots for decomposition of the precursor microemulsion products (i.e. zinc glycerolate particles) for two microemulsion formulations: (a) ME-I and (b) ME-II.

diffractions. The JCPDS card of crystalline ZnO is also presented as an inset in Fig. 1 for comparison purposes and shows the relative intensities for the possible diffractions. For all calcination treatments, the diffraction peak intensities of the ZnO product of ME-I show a better match with the standard card in terms of intensity order for the diffraction events. The XRD patterns of ZnO particles, synthesized in ME-II systems and calcined at 300 or 400 °C, on the other hand show a distinct deviation from the standard pattern in relative intensities of the observed diffractions. For the ZnO powder of ME-II, calcined at 500 °C, the diffraction peak intensities and their order are again in agreement with standard card intensities. The reasons for such differences will be further clarified in Section 4.

TGA-DSC results of the microemulsion products of ME-I and ME-II are shown in Fig. 2a and b, respectively. Measurements were performed for the samples in as-prepared condition which were heated from 30 to 700 °C in air. According to TGA curves of ME-I and ME-II, there is a very small amount of weight loss (around 2 wt.%) up to 200 °C. The broad exothermic events (280–450 °C) in DSC curves are attributed to decomposition of Zn-Gly complex to ZnO and crystallization of ZnO particles. The DSC and TGA data are somewhat in agreement with each other, as the temperatures of the broad exothermic peak coincide with the temperature ranges of the main weight loss. However, the DSC curves show two exothermic peaks. The first sharp peak at around 340 °C corresponding to the main weight loss in TGA curves is attributed to the decomposition of Zn-Gly particles to ZnO. The second exothermic peak indicates that there must be another reaction such as volatilizing, combustion of organics accompanying the decomposition of Zn-Gly [30]. Absence of weight loss or heat flow change above 450 °C indicates that no reaction takes place beyond 450 °C.

Fig. 3 illustrates the SEM micrographs of ZnO particles of ME-I system after calcination for 3 h at 300, 400 and 500 °C. The ZnO nanoparticles exhibit a spherical morphology with a narrow and uniform size distribution. The average particle size varies in the range of 15–25 nm and increases with calcination temperature within the temperature range of the study, i.e. 300–500 °C. Calcination at 500 °C also initiates neck formation between the particles as shown in Fig. 3. SEM micrographs of microemulsion products after same calcination treatments for ME-II are presented in Fig. 4. Particles of ME-II calcined at 300 and 400 °C exhibit a distinctly different morphology compared to those for ME-I and have a rod-like morphology again with a narrow size distribution. The length of the rods is approximately 65–70 nm, with a typical diameter of 22–28 nm. ZnO particles of ME-II calcined at 500 °C on the other hand have a spherical morphology as shown in Fig. 4 with an average particle size of 22 nm. The average particle sizes of the ZnO powders determined from SEM examinations are listed in Table 1, together with the crystallite size values estimated by Scherrer's equation.

Fig. 5 shows the PL spectra of ZnO nanoparticles obtained for ME-I and ME-II formulations calcined at different temperatures. As shown in Fig. 5a, the PL spectra of ME-I products consists of a weak UV-emission peak (385 nm) as illustrated in the inset of the figure and strong deep-level green emission peak (530 nm). The intensity of weak UV-emission band decreases with increasing calcination temperature but the intensity of strong green emission increases with calcination temperature. Fig. 5b presents PL spectra of ME-II products. There is only strong deep-level green emission peak and it becomes stronger with increasing calcination temperature resulting in an enhanced green emission.

4. Discussion

A reverse microemulsion system has been employed to synthesize ZnO nanoparticles with different size and morphology. A water-in-oil microemulsion acting as a binary aqueous nanoreactor system for Zn-complex formation was obtained when glycerol droplets are surrounded by AOT surfactant molecules in n-heptane (oil phase). In such a water-in-oil microemulsion system; AOT dissolves in the dispersed phase and form stable micelles reach in Na^+ ions. When Zn^{2+} ions are incorporated ion exchange reaction takes place and finally Na^+ replaces with Zn^{2+} in the dispersed micelles [1]. The Zn-Gly complex acting as a precursor for ZnO formation

Table 1
Average crystallite size estimated from the XRD results and average particle size as determined from SEM examinations for the ZnO nanoparticles calcined at different temperatures.

Microemulsion formulation	ME-I		ME-II	
Calcination temperature	Average crystallite size (XRD)	Average particle size (FESEM)	Average crystallite size (XRD)	Average particle size (FESEM)
300 °C	16.4 nm	15 ± 1 nm	n.a.	*d*: 22 ± 3 nm *l*: 66 ± 3 nm
400 °C	28.8 nm	18 ± 0.5 nm	41 nm	*d*: 28 ± 1 nm *l*: 72 ± 1 nm
500 °C	26.8 nm	24 ± 1 nm	31.7 nm	21.6 ± 1 nm

n.a., not available; *d*, diameter; *l*, length.

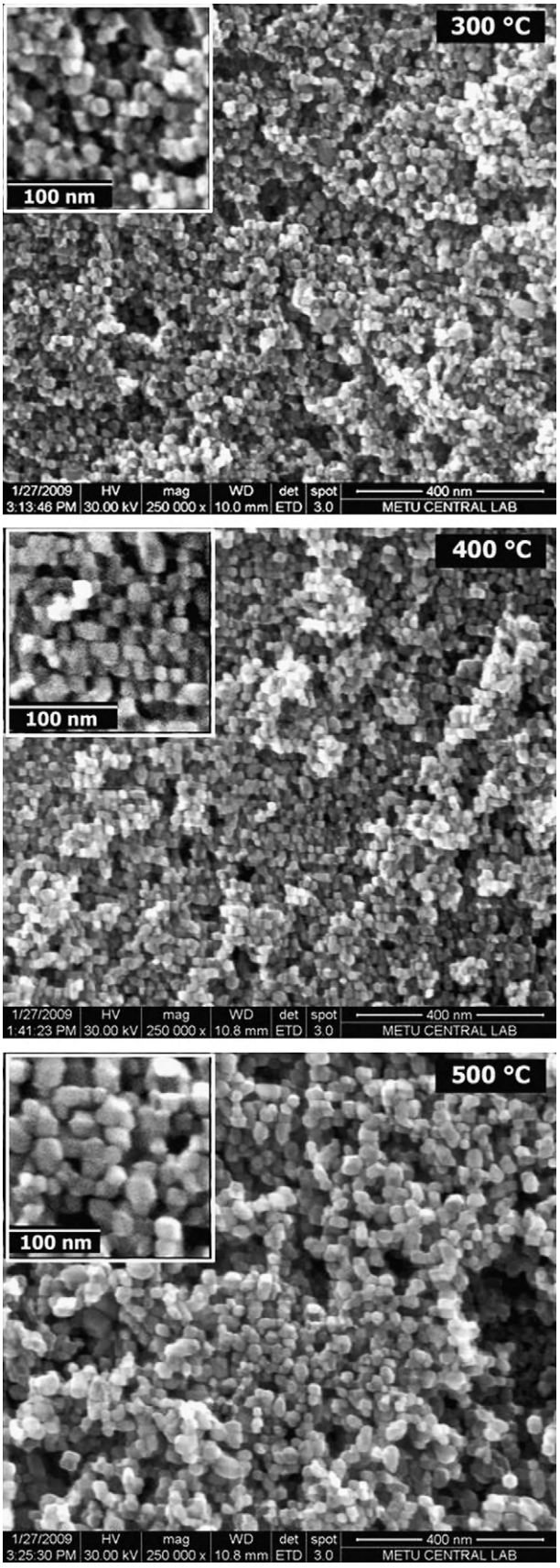

Fig. 3. SEM micrographs of the ZnO nanoparticles of the microemulsion ME-I calcined at 300, 400 and 500 °C. The insets are the segments from the underlying SEM images magnified twice as a visual aid indicating dimensional details.

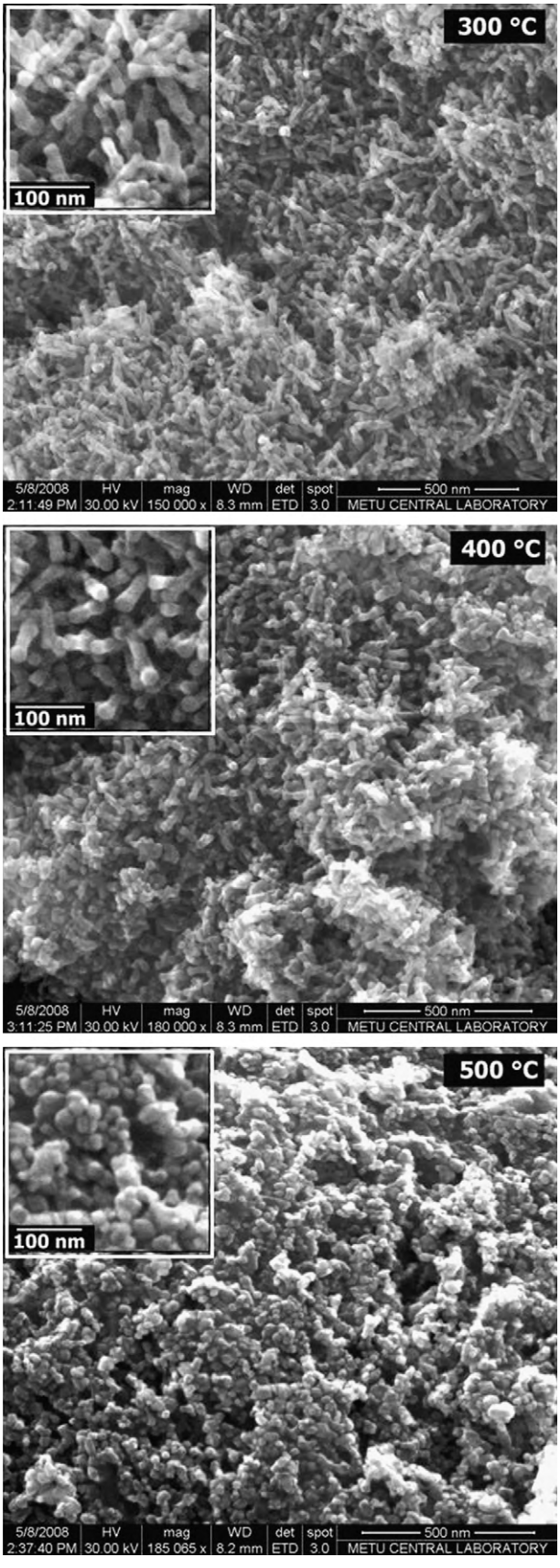

Fig. 4. SEM micrographs of the ZnO nanoparticles of the microemulsion ME-II calcined at 300, 400 and 500 °C. The insets are the segments from the underlying SEM images magnified twice as a visual aid indicating dimensional details.

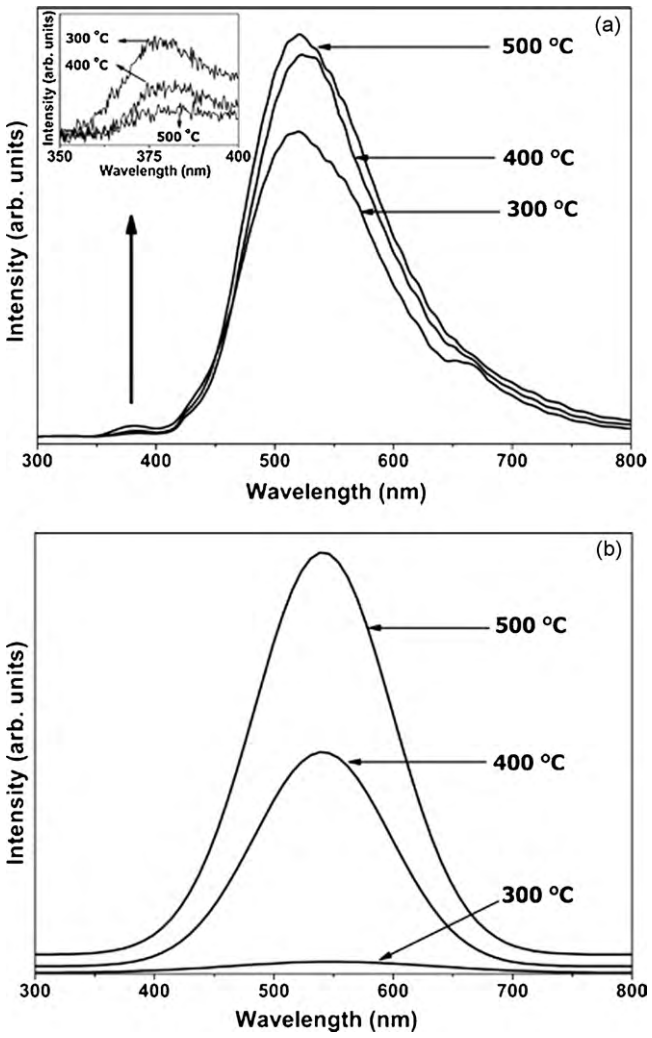

Fig. 5. Room temperature PL spectra of the ZnO nanoparticles calcined at 300, 400 and 500 °C for two microemulsion formulations: (a) ME-I and (b) ME-II.

was synthesized in the presence of NaOH, because the reaction between zinc acetate and glycerol is much faster in basic environment and as Zn-Gly decomposes in acidic solutions [31]. In other words, NaOH was used as electrolyte serving for glycerol stabilization in n-heptane and provides rigidity for the droplet interfacial film and so the stability of droplet size [32]. As can be noted from the XRD and thermal analyses, formation of ZnO originates from the decomposition of Zn-Gly complex precursor, whose morphology is most likely controlled by the shape of the nanoreactors in the microemulsion system which does not change their shape during thermal decomposition to ZnO. In this sense nucleation and growth of ZnO crystals occur in the definite shape of this precursor upon subsequent thermal treatment.

One obvious effect of surfactant amount in the studied microemulsion system is on particle morphology. Higher surfactant concentration results in rod-like nanoreactors and eventually rod-like ZnO products as can be seen for the ME-II microemulsion products calcined at 300 and 400 °C. Formation of rod-like nanoreactors in the presence of higher amount of surfactants is analogous to that reported by others [29,33]. As shown by the schematics in Fig. 6, a low surfactant concentration beyond critical micelle concentration favors the formation of spherical water-in-oil droplets, so formation of spherical ZnO particles as in the case of ME-I. Whereas higher surfactant concentration favors development of interconnected cylindrical droplets, and generates rod-like ZnO particles as in the case of ME-II. This compositional modification in the microemulsion formulation in fact gives a chance to control the final particle morphology at nano-scale.

Another finding related with the physical difference for two microemulsion products is the change in the average particle size and morphology with the calcination temperature. For all calcination temperatures, the ZnO powders of ME-I microemulsion formulations are typically spherical and exhibited bigger sizes with increasing calcination temperature. Similar observations have also been reported by other researchers [34]. On the other hand, ME-II microemulsion products after calcination at 300 and 400 °C had a rod-like morphology and exhibited a structural rod-to-sphere shape transformation at higher calcination temperatures (500 °C). While the SEM observations clearly demonstrate such differences, the XRD data also provide indirect evidence. The intensity order of the diffractions of the ZnO products of ME-I shows a complete match with the intensities listed standard JCPDS card (No. 36-1451) data, which corresponds the most random arrangement of crystal planes for powder crystal sample. The ideal intensity order, corresponding to most random crystal arrangement is actually presentation of the thermodynamically most stable form which can be approximated by spherical morphology. ZnO products of ME-II calcined at 300 and 400 °C, however, show some deviation from the standard intensity order; and have relatively more intense (0 0 2) diffraction peaks (as shown in Fig. 2b) compared to standard card data. (0 0 2) direction is the *c*-axis of the hexagonal ZnO crystal. This indicates presence of preferred crystallographic orientation, here a rod-like, of ZnO crystals for this particular microemulsion formulation with higher amount of surfactant.

The observation regarding the calcination temperature dependent structural rod-to-sphere shape transformation most likely results from size and defect controlled thermodynamic factors. It has been reported that gold nanorods can be transformed into sphere-like nanoparticles by photo induced processes leading to a thermal excitation resulting high defect generation and allowing a shape transformation to the energetically more stable spherical shape [35]. Similar transition for ZnO nanorods may occur by thermal means during calcination at relatively higher temperatures (500 °C). In ZnO unit lattice, Zn terminated top surfaces (0 0 0 1) are catalytically active, while O terminated bottom surfaces are catalytically inert. Each Zn and O atoms are arranged alternatively along the *c*-axis. Due to catalytically and energetically active top surfaces, the preferred growth occurs along this direction [36]. In our case, ME-II microemulsion formulation yields to rod-like ZnO products after calcination 300 and 400 °C, and shape transition to spherical nanoparticles occurs at higher temperatures (500 °C). As revealed by distinctly increasing green emission for the ZnO products, the system reaches to excessively high defect concentration upon calcination 500 °C. This defect associated excessive energy induces such shape transition to eliminate highly energetic facets by taking spherical form.

Increasing calcination temperature also affect the particle size of the rod-like ZnO powders of ME-II as shown in Fig. 4. Lu et al. studied microemulsion mediated hydrothermal synthesis of TiO_2 particles [37]. They showed that the aspect ratio of rod-like TiO_2 particles decreases with an increase in synthesis temperature. In the present study, same behavior in the size of rod-like ZnO particles has been observed as a result of increasing calcination temperature. While length and diameter of the rod-like ZnO particles increase from 66 ± 3 and 22 ± 3 nm to 72 ± 1 and 28 ± 1 nm, respectively, the aspect ratio (length/diameter) of the rod-like ZnO nanoparticles decreases from 3.0 to 2.6 with an increase in calcination temperature from 300 to 400 °C. This decrease in aspect ratio again implies a morphological approximation to a more equiaxed shape with increasing calcination temperature.

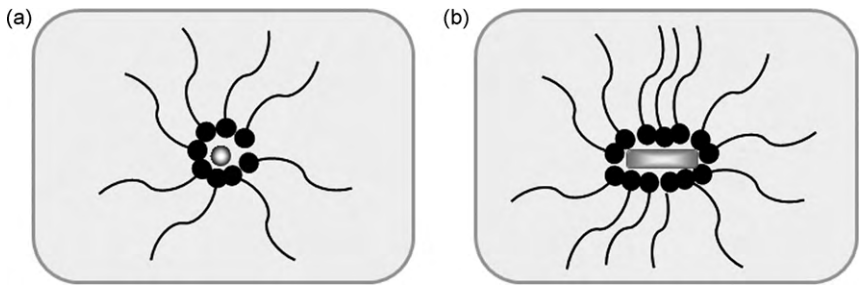

Fig. 6. Schematic illustration for the formation of different ZnO morphologies: (a) in microemulsion formulation ME-I that has low surfactant amount and (b) in microemulsion formulation ME-II containing a higher surfactant content.

In regard to optical properties, the relatively weak UV-emission peak at around 385 nm attributed to the exciton combination emission indicates a passivated surface for the ZnO nanoparticles. The quenching of UV-emission may be due to surface defects in the form of OH groups [38,39]. The strong deep-level green emission at around 530 nm resulting from the defects associated with oxygen vacancies or zinc interstitials implies a populated defect concentration for ZnO crystals of both microemulsion products ME-I and ME-II. A higher calcination temperature enhances the green emission intensity suggesting a correlation between green emission and isolated oxygen vacancies as proposed by others [40]. With increasing calcination temperature; the kinetic energy of atoms in ZnO lattice will increase and the escape rate of oxygen atoms from ZnO lattice will be faster than rate of getting oxygen atoms to lattice [41] resulting in more vacancy formation and higher green emission.

5. Conclusions

ZnO nanoparticles have been synthesized by a modified reverse microemulsion comprised of Aerosol OT, acting as surfactant, and glycerol, serving as water phase. By employing glycerol as an internal phase in the microemulsion formulation, it was possible to obtain an intermediate zinc-complex rather precipitation of ZnO crystals as the microemulsion product. This prevented formation agglomerated ZnO products. The intermediate Zn-Gly complex was converted to ZnO by thermal decomposition during subsequent calcination. In this way monodispersed and spherical ZnO nanoparticles with average particle size of 15 nm were successfully obtained. The particle size of the spherical ZnO nanoparticles could be controlled by changing calcination temperature, i.e. 15 ± 1 nm (when calcined at 300 °C), 18 ± 1 nm (at 400 °C) and 24 ± 1 nm (at 500 °C). Hence, the proposed microemulsion system is advantageous for obtaining size controlled ZnO nanoparticles with narrow size distribution. Additionally, the proposed microemulsion system also allows attaining variation in ZnO morphology which can be achieved by changing the surfactant amount in the microemulsion formulation. Higher surfactant concentrations and calcination temperatures not exceeding 400 °C promotes formation of rod-like ZnO microemulsion products with typical diameters and lengths of 25 and 60–70 nm, respectively. The findings of the study indicated that the suggested modified microemulsion method provides an alternative approach for synthesis of ZnO nanoparticles by a simple wet chemical route which enables tailoring the size and morphology of the ZnO nanoparticles.

Acknowledgements

This work is supported through Middle East Technical University Grant No. BAP-03-08-07. ÖAY also thank The Scientific and Technological Research Council of Turkey, TUBITAK, for the support through National Scholarship Program for PhD students and also METU-ÖYP Program. The authors wish to thank M. Vedat Akdeniz for the assistance in thermal analyses and Raşit Turan for PL measurements.

References

[1] M. Singhal, V. Chhabra, P. Kang, D.O. Shah, Mater. Res. Bull. 32 (1997) 239–247.
[2] H.Y. Liu, H. Kong, X.M. Ma, W.Z. Shi, J. Mater. Sci. 42 (2007) 2637–2642.
[3] K.S. Weissenrieder, J. Müller, Thin Solid Films 300 (1997) 30–41.
[4] Q. Wan, Q.H. Li, Y.J. Chen, T.H. Wang, X.L. He, J.P. Li, C.L. Lin, Appl. Phys. Lett. 84 (2004) 3654–3656.
[5] C.D. Lokhande, P.M. Gondkar, R.S. Mane, V.R. Shinde, S.-H. Han, J. Alloy Compd. 475 (2009) 304–311.
[6] Y.B. Li, Y. Bando, D. Golberg, Appl. Phys. Lett. 84 (2004) 3603–3605.
[7] R.C. Wang, C.P. Liu, J.L. Huang, S.-J. Chen, Y.-K. Tseng, S.-C. Kung, Appl. Phys. Lett. 87 (013110) (2005) 1–3.
[8] H. Rensmo, K. Keis, H. Lindström, S. Södergren, A. Solbrand, A. Hagfeldt, S.-E. Lindquist, L.N. Wang, M. Muhammed, J. Phys. Chem. B 101 (1997) 2598–2601.
[9] C. Lin, H. Lin, J. Li, X. Li, J. Alloy Compd. 462 (2008) 175–180.
[10] L. Wang, M. Muhammed, J. Mater. Chem. 9 (1999) 2871–2878.
[11] R. Hong, T. Pan, J. Qian, H. Li, Chem. Eng. J. 119 (2006) 71–81.
[12] F.D. Paraguay, W.L. Estrada, D.R.N. Acosta, E. Andrade, M. Miki-Yoshida, Thin Solid Films 350 (1999) 192–202.
[13] T. Tani, L. Madler, S.E. Pratsinis, J. Nanopart. Res. 4 (2002) 337–343.
[14] J. Wang, L. Gao, J. Mater. Chem. 13 (2003) 2551–2554.
[15] B. Liu, H.C. Zeng, J. Am. Chem. Soc. 125 (2003) 4430–4431.
[16] U. Pal, P. Santiago, J. Phys. Chem. B 109 (2005) 15317–15321.
[17] L. Spanhel, M.A. Anderson, J. Am. Chem. Soc. 113 (1991) 2826–2833.
[18] M. Ristic, S. Music, M. Ivanda, S. Popovic, J. Alloy Compd. 397 (2005) L1–L4.
[19] H.M. Cheng, H.C. Hsu, S.L. Chen, W.T. Wu, C.C. Kao, L.J. Lin, W.F. Hsieh, J. Cryst. Growth 277 (2005) 192–199.
[20] Y.Y. Tay, S. Li, F. Boey, Y.H. Cheng, M.H. Liang, Physica B 394 (2007) 372–376.
[21] S. Hingorani, V. Pillai, P. Kumar, M.S. Multani, D.O. Shah, Mater. Res. Bull. 28 (1993) 1303–1310.
[22] C.H. Lu, C.H. Yeh, Mater. Lett. 33 (1997) 129–132.
[23] R. Moleski, E. Leontidis, F. Krumeich, J. Colloid Interface Sci. 302 (2006) 246–253.
[24] M. Inoguchi, K. Suzuki, K. Kageyama, H. Takagi, Y. Sakabe, J. Am. Chem. Soc. 91 (2008) 3850–3855.
[25] L. Guo, Y.L. Ji, H.B. Xu, P. Simon, Z.Y. Wu, J. Am. Chem. Soc. 124 (2002) 14864–14865.
[26] Y. Liu, Z. Liu, G. Wang, J. Cryst. Growth 252 (2003) 213–218.
[27] T. Ahmad, S. Vaidya, N. Sarkar, S. Ghosh, A.K. Ganguli, Nanotechnology 17 (2006) 1236–1240.
[28] Y. Lv, L. Guo, H. Xu, L. Ding, C. Yang, J. Wang, W. Ge, S. Yang, Z. Wu, J. Appl. Phys. 99 (114302) (2006) 1–4.
[29] X. Li, G. He, G. Xiao, H. Liu, M. Wang, J. Colloid Interface Sci. 333 (2009) 465–473.
[30] Y. Yang, H. Chen, B. Zhao, X. Bao, J. Cryst. Growth 263 (2004) 447–453.
[31] D.P. Fairlie, M.W. Whitehouse, R.M. Taylor, Agents Actions 36 (1992) 152–158.
[32] D.J. Liu, J.M. Ma, H.M. Cheng, Z.G. Zhao, Colloid Surf. A 143 (1998) 59–68.
[33] G. Sun, M. Cao, Y. Wang, C. Hu, Y. Liu, L. Ren, Z. Pu, Mater. Lett. 60 (2006) 2777–2782.
[34] Y.J. Kwon, K.H. Kim, C.S. Lim, K.B. Shim, J. Ceram. Process. Res. 3 (2002) 146–149.
[35] S. Link, Z.L. Wang, M.A. El-Sayed, J. Phys. Chem. B 104 (2000) 7867–7870.
[36] P.X. Gao, Z.L. Wang, J. Phys. Chem. B 108 (2004) 7534–7537.
[37] C.-H. Lu, W.-H. Wu, R.B. Kale, J. Hazard. Mater. 154 (2008) 649–654.
[38] H. Zhou, H. Alves, D.M. Hofmann, W. Kriegseis, B.K. Meyer, G. Kaczmarczyk, A. Hoffmann, Appl. Phys. Lett. 80 (2002) 210–212.
[39] H.K. Yadav, K. Sreenivas, V. Gupta, S.P. Singh, R.S. Katiyar, J. Mater. Res. 22 (2007) 2404–2409.
[40] K. Vanheusden, C.H. Seager, W.L. Warren, D.R. Tallant, J. Caruso, M.J. Hampden-Smith, T.T. Kodas, J. Lumin. 75 (1997) 11–16.
[41] X.Q. Meng, D.Z. Shen, J.Y. Zhang, D.X. Zhao, Y.M. Lu, L. Dong, Z.Z. Zhang, Y.C. Liu, X.W. Fan, Solid State Commun. 135 (2005) 179–182.